SINDH UNIVERSITY RESEARCH JOURNAL (SCIENCE SERIES)
ISSN (Print) 1813-1743, ISSN (online) 2791-0547
Vol. 54 No 04 (2022)
Doi: https://doi.org/10.26692/surj-ss.v54i04.6127

An Estimation of the Land Surface Temperature, Derived from the Landsat Satellite, for the Major Cities in Sindh Province, Pakistan

MEHJABEEN KHAN[1], IRFAN AHMED SOOMRO[2]*, ZAEEM HASSAN AKHTER[3], SUJO MEGHWAR[4], MUMTAZ ALI LAKHO[5]

[1]Department of Physical Geography, Nanjing University, Nanjing, Jiangsu 210023, China.
[2]Key Laboratory of Ocean and Marginal Sea Geology, Innovation Academy of South China Sea Ecology and Environmental Engineering, South China Sea Institute of Oceanology Chinese Academy of Sciences, Guangzhou 511458, China.
[3]School of Geography, Nanjing Normal University, Nanjing, Jiangsu, China.
[4]Department of Geography, University of Sindh, Jamshoro
[5]Deputy Director Geological Survey of Pakistan, Quetta, Pakistan.

Cite this:
Mahjabeen K, IA. Soomro, ZH. Akhtar, S. Meghwar, and MA Lakho (2022). An estimation of the land surface temperature, derived from the Landsat satellite, for the major cities in Sindh Province, Pakistan. Sindh Uni. Res.J. (SS) **54:4** (2022).

Corresponding author
geographerirfan@gmail.com

Abstract

Thermal infrared remote sensing data are used to make estimates of the land surface temperature (LST) by recording the radiant energy emitted by the surface of the Earth. Satellite data and image processing software also allow for LST estimation. Since its launch, two thermal infrared bands aboard the Landsat satellite have been used to continuously observe Earth, providing data for the estimation of LST and the normalized difference vegetation index (NDVI). Due to the significant uncertainty in data from both Landsat 5 thematic mapper (TM) thermal band 6, which has a wavelength of 10.40–12.50 m, and Landsat 8 thermal infrared sensor (TIRS) Band 11, as indicated by USGS calibration notifications, it was advised to use TIRS Band 10 data as a single spectral band for LST estimation. For LST estimation from Landsat 5 and Landsat 8, the mono-window (MW) approach was used with TM and TIRS Bands 6, 10, and data with a resolution of 120 and 100 m. (Path-152 and Row-40, 41, 42, and 43). The emission coefficient was calculated using the operational land imager (OLI) Bands 4 and 5 (30 m resolution) and the normalized difference vegetation index (NDVI) proportion of vegetation method. Based on the results, the LST was higher in the arid regions, whereas the NDVI was higher in the less arid parts. Also, the LST findings were compared to the air temperature data, both data were found to be consistent with one another. The approach of MW algorithm could be a useful tool for estimating LST from TM data acquired from Landsat 5 and Landsat 8 TIRS Bands 6 and 10.

Keywords: Satellite, Landsat 5, Landsat 8, LST, NDVI, and Sindh

Introduction

Information about an object can be gathered via the electromagnetic spectrum through a process called "remote sensing," which does not require direct contact with the thing being investigated. Recent decades have seen a boom of applications for high-tech satellite data in the study of environmental phenomena and climatic change. The temperature of the Earth's land surface can be accurately determined with the use of data gathered from the thermal bands of Landsat 5 and Landsat 8 LST. Microclimate and atmospheric radiation transport are two areas where it has been found to play a significant role (Mauree, et al. 2019).

The area's LULC (land use/land cover) is also a major consideration in LST estimation. The LST of a region is affected by changes in the physical and biological conditions brought about by both natural and human-caused processes. When the value of LST shift changes, the weather pattern in that region shifts, too (Brown, et al. 1986, Duveiller, et al. 2018). Traditional methods of estimating surface temperatures, for some types of terrain conditions, such as monitoring by a meteorological department weather station and other public and private sector observation methods, are not viable and also take time. Remote sensing satellites, on the other hand, can provide information on a region's topography and climate, including the unique local climates (microclimates) formed by changing land surfaces. The National Aeronautics and Space Administration (NASA) The Landsat program offers satellite Images with varying spatial resolutions for a range of time frames. Thematic mapper for Landsat 5 images (TM), which has seven bands with (30-m resolution). For more precise surface temperature images, Landsat 8 takes two sets of images: one from OLI with nine bands (30-m resolution) and another from TIRS with two bands (Band 10 and Band 11 with 100-m resolution) (Wulder, et al. 2019). The TIRS detects infrared light with very long wavelengths by observed quantum well-infrared photodetectors (QWIPs). The temperature of the earth's surface determines the intensity of this light. The normalized difference vegetation index (NDVI) analysis is a great way to estimate LST in mountainous areas like the Himalayan and Karakorum (K2) ranges. This is because surface temperatures are directly related to the physical properties of the surface.

Integration of the temperature on the land surface is a crucial variable that has been recognized as being important for the investigation of atmospheric radiation transfer and microclimate. The surface temperatures of the soil, water content, and plants are referred to as LST (Yu, et al. 2011).

Hokao, et al. (2012) examined the relationship between LST and NDVI using the thermal features of Bangkok's rapidly urbanizing metropolitan area were determined using Landsat thematic mapper (TM) data from 1994, 2000, and 2009. Their research showed a strong correlation between LST and NDVI in several types of LULC, especially in forested regions. The effects of urbanization on LST were primarily caused by a decline in biomass. Similar recommendations were made by (Li, et al. 2004, Giannini, et al. 2015, Awuh, et al. 2019) utilizing high-resolution sequence satellite data, to conduct an LST analysis over a watershed area located in Lowa, Bangkok. Scene for the LST was taken from the thermal bands of Landsat 5 TM and Landsat 7 ETM. The NDVI was computed from the visible and near-infrared (Band 4 and Band 5) bands of the satellite to estimate emissivity for Landsat thermal bands. In this study, predicted LST values were compared to actual observations. When comparing LST to estimates derived from Landsat 5 and 7, as well as the actual measurements taken on the ground, a range of discrepancies between 0.98 and 1.47 degrees Celsius was discovered. Satellite images were used to pinpoint the locations of LST deviations. Another study used Landsat TIRS and OLI data to calculate the LST variation over hiruvananthapuram, the capital of Kerala, India (Dagliyar, et al. 2015). Using open- source GIS software conglomeration quantum (QGIS), which is able to acquire images, process them, categorize land covers, and derive LST from the land's surface using the study's findings. Based on measurements of surface emissivity and brightness, With a 12-bit radiometric resolution and Landsat 8 OLI and TIRS, we were able to determine LST for urban Erzurum. Kinetic surface temperature measurements from the general directorate of the state meteorological service in and around the study area were used to partially validate the Landsat 8 bands' LST. According to the findings, the highest temperature difference recorded was about 6.45 degrees Celsius, while the smallest was about 1.86 degrees Celsius.

In this research work also, LULC and LST, which were obtained from Landsat 5 and Landsat 8, a temperature difference seen. Additionally, research by (Cao, et al. 2008, Lv and Zhou 2011, Makinde and Obigha 2017, Ning, et al. 2018) we were able to establish the relationship between LULC change and LST using Landsat 5 TM and ETM images. The object-based approach was utilized to derive the land use classification. After obtaining LST, the MW algorithm was applied. The conclusions reached showed that the LULC had a considerable impact on LST. It was also discovered that LST has a positive correlation with impervious surface.

Results from these studies indicated that rapid urbanization was an area where this type of research would be most useful. Recently, in Devikulam taluk, LST was estimated using 1990, 2001, and 2010 Landsat 5 TM and Landsat ETM data by following the instructions in the Landsat 7 user handbook where described in detailed (Suga, et al. 2003, De Jesus and Santana 2017). The results indicated a steady rise in average temperature (Allen, et al. 2018). According to the research on climate change, land surface temperature (LST) is a major factor that

must be taken into consideration. Estimating the LST's accuracy with modern satellite data (like Landsat 5 and Landsat 8) is also crucial as it has a direct impact on precision. But the TM and advanced TIRS data have been used in very few studies thus far both Landsat 5 and Landsat 8 TM and TIRS data were used to analyze the MCS and calculate LST for this study.

The aim of this study is to (1) asses the spatiotemporal distribution and variations in LSTs, to contribute towards the development of sustainable management plans curbing local and global climate change impacts, (2) To assess the accuracy of Landsat products using air temperatures from climate data of MCS, and (3) Explore the distribution and spatiotemporal variation characteristics of LSTs and the associated main land surface.

Materials and Methods

Region of Interest

The study area includes major cities of Sindh (MCS), which is Sindh province of Pakistan (Figure 1), with the names Hyderabad (HYD), Jacobabad (JCB), Jamshoro (JAM), Karachi (KHI), Larkana (LRK), Matari (MAT), Noshero Feroz (NF), Shaheed Benazirabad (SBB), Shikarpur (SHP), and Thatta (THAT). The location of the study area lies between 28° 43′ 43″ and 23° 94′ 33″ N latitude and 66° 65′ 13″ and 69° 05′ 86″ E longitude as depicted and covers an area of 40584 km2. The area of study in the north region has plain land, whereas the south part has small hills and barren land. The Indus River crosses the MCS, which originates in Tibet and follows a circuitous route southward through the Himalaya Mountains to the Arabian Sea, emptying into the ocean southeast of the coastal city of Karachi. The river is mostly fed by snowmelt during the summer season. The river basin receives a significant amount of precipitation over the monsoon season, which usually takes from July to the end of August. It does this by soaking up the moisture carried on the breezes from the Arabian Sea as well as other sources. During the winter months, snowfall can be found in the upper portion of the river.

The images from Landsat 5 and Landsat 8 have already been rectified to WGS-1984-UTM-Zone_42N. After that, the metadata file and the thermal band at satellite brightness temperature (TB) were used to convert the digital number (DN) to the physical measure of top of atmospheric (TOA) reflectance. The thermal constants required to convert TM, TIRS data using satellite TB were later made available in a file with the extension ". MTL" that was included in the Landsat 5 and Landsat 8 image set. Finally, the spectral radiance was converted to TB using the thermal and TIRS band data and the thermal constants listed in the metadata file (Table 1 to 2).

Table 1. Landsat 5 and Landsat 8 Metadata of the study area captured at a resolution of 30 meters.

Satellite/ sensor	Date Acquisition	Band	Path/Row
LANDSAT-5 TM	03/06/2011	7	152/40
			152/41
			152/42
			152/43
LANDSAT-8 OLI/TIRS	13/05/2021	11	152/40
			152/41
			152/42
			152/43

Table 2. K1 and K2 Values

Sensor	K1	K2	Thermal Band
Landsat 5 TM	607.76	1260.56	6
Landsat 8 / OLI/TIRO	774.89	1321.08	10.11

Acquisition of data

In this study, Landsat 5 and Landsat 8 image of 03 June, 2011 and 13 May, 2021 (Path/Row - 152/40, 41, 42 and 43) cloud free downloaded, the NDVI and LST were calculated using data from the study area. A topographical map of the study area at 30 m spatial resolution, obtained from the USGS earth explorer website https://earthexplorer.usgs.gov/. The topographical image from U.S. Geological Survey (USGS), U.S. Environmental Protection Agency (EPA) http://server.arcgisonline.com/ArcGIS/rest/services/. The climate data include, air temperature data were acquired from the Climate Data Processing Centre (CDPC), Pakistan Meteorological Department (http://www.pmd.gov.pk/), the climate data included ten MCS such as HYD, JCB, JAM, KHI, LRK, MAT, NF, SBB, SHP and THAT located within the study area (Figure 1).

This analysis, summarized in Table 1, made use of information gathered by the Landsat 5 Thematic Mapper (TM) in 2011 and the Landsat 8 Operational Land Imager (OLI) and Thermal Infrared Sensor (TIRS) in 2021. Furthermore, ArcMap 10.4 software is used for mosaic and area of interest (AOI)

extraction. Normalized differential vegetation index (NDVI) and land surface temperature (LST) indices are calculated for 2011 and 2021. The development of the surface temperature profile also makes it possible to identify the study areas with the highest and lowest average surface temperatures. In addition, the NDVI and LST are retrieved by making use of the clip tools that are available in the ArcGIS 10.4 software. The (Figure 2) provides an overview of a comprehensive description of the process.

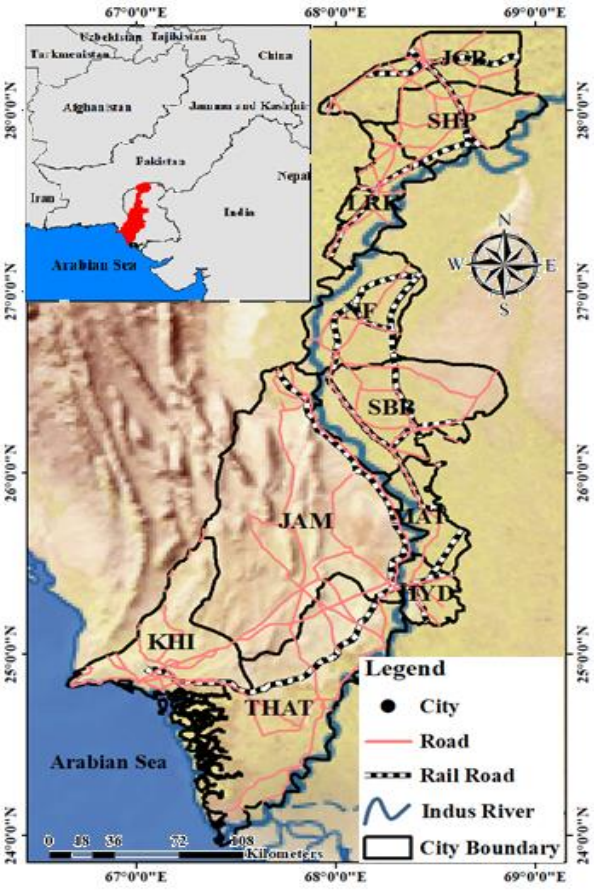

Figure 1. The map display study area and MCS boundaries

NDVI

Equation 1 proposed by (Gao, 1996; Jarchow, Nagler, & Glenn, 2017) can be calculated using Landsat data (specifically the red and infrared bands). Because chlorophyll absorbs light most strongly in the near-infrared and red bands of the electromagnetic spectrum, the ratio of these two regions is used for the calculation (Kumari, Tayyab, Mallick, Khan, & Rahman, 2018).

$$NDVI = \frac{\text{NIR} - \text{Red}}{\text{NIR}+\text{Red}} \qquad (1)$$

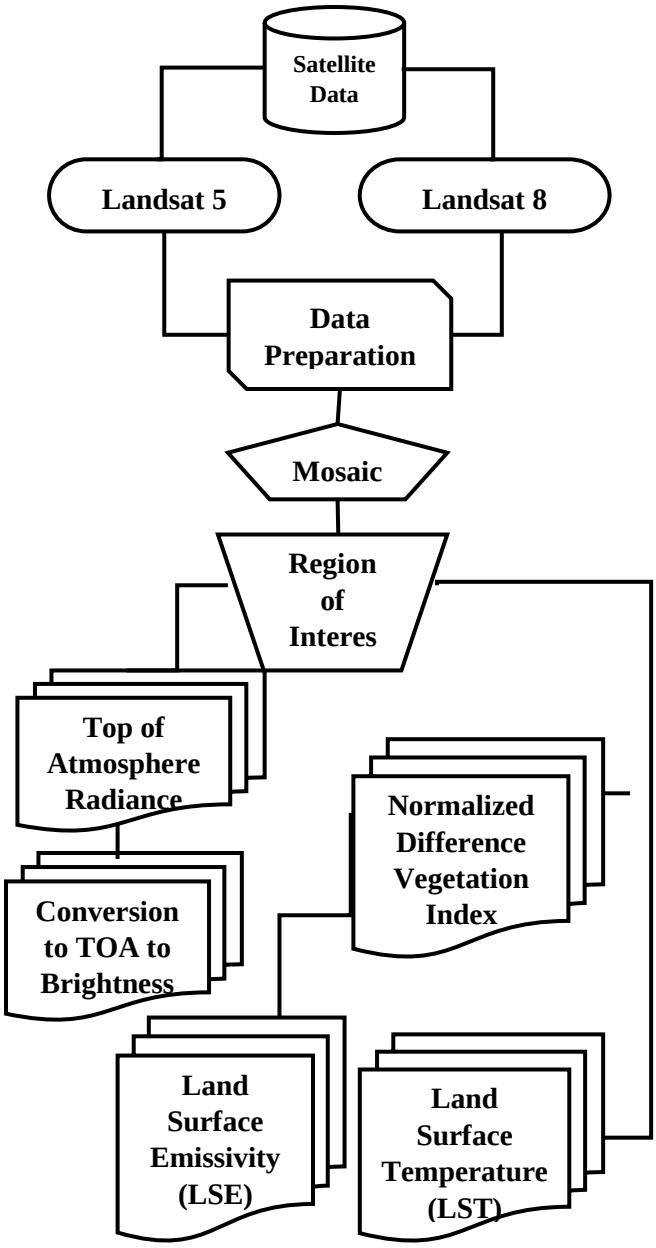

Figure 2. Flow chart of the Landsat 5 and Landsat 8 used to analysis.

LST

Retrieval of LST for Landsat 5 MSS + TM

This study uses the retrieval of surface temperature from Landsat 5 data, as described in the Landsat 5 manual, to derive LST. The following are the procedures for determining LST.

Equation 2 is used to transform the image's digital number into spectral radiance.

$$L\lambda = \left(\frac{LMax\lambda - LMin\lambda}{Qcal Max - QcalLMin}\right) \times (Qcal - QaclMin) + LMin\lambda \qquad (2)$$

Second, using Equation 3, we transform the radiation brightness into the at-satellite brightness temperature, T Kelvin (K).

$$T = \frac{K2}{\ln\left(\frac{K1}{L\lambda}+1\right)} \quad (3)$$

Where:
K1 = 1260.56 and K2 = 607.66 (mW$^{\times}$cm-2$^{\times}$ sr-1) which were used as reference points before the launch: A sensor's response of more than 50% indicates an effective spectral range represented by. b = 1.239 (µm).

Retrieval of LST for Landsat 8 OLI/TIRS

This research relies on the retrieval of surface temperature from Landsat 8 data, as detailed in the Landsat 8 handbook, to derive LST.
Metadata radiance rescaling factors are used in Equation 4 to first convert OLI and TIRS band data to radiance.

$$L\lambda = MLQcal + AL \quad (4)$$

Where:
L_{λ}=Temperature of atmosphere spectral radiance
M_L =band-specific multiplicative rescaling factor from the metadata (Radiance multi band X where X is the band number)
A_L=band-specification additive rescaling factor from the metadata (radiance add band X, where X is the band number)
Qcal=quantized and calibrated standard product pixel values (DN)

At this step, the reflectance rescaling coefficients from the product metadata file are used to transform the band data into reflectance (MTL file). For OLI data, the DN value is converted to TOA reflectance using Equation 5.

$$\rho\lambda = M\rho Qcal + A\rho \quad (5)$$

Where:
$\rho\lambda$ = reflectance
M_{ρ}= band-specific multiplicative rescaling factor from the metadata (reflective multi band x, where x is the band number)
Qcal= quantized and calibrated standard product pixel values (DN)

Third, using the thermal constants listed in the metadata file and Equation 6, spectral radiance data from the TIRS band is converted to brightness temperature.

$$BT = \frac{K2}{In\left[\left(\frac{K1}{L\lambda}\right)+1\right]} \quad (6)$$

Where:
T = at-satellite brightness temperature (K)
Lλ= residence
Where:
The thermal conversion constants K1 and K2 are defined in the metadata and correspond to the band specifications. By recalculating the radiant temperature with Equation 7, applied to convert the results to Celsius.

$$T\ (^{o}C) = T(K) - 273.15 \quad (7)$$

NDVI Method for Emissivity Correction

The normalized difference vegetation index (NDVI) was determined using the visible and near-infrared bands from Landsat (Eq. 1). Due to the fact that the amount of vegetation is a significant component in determining LST, assessing the NDVI is paramount (Sekertekin & Bonafoni, 2020); Next, we use NDVI to evaluate the vegetation fraction (Pv) (Equation 8).

$$P_v = (NDVI - NDVI_{Min})/(NDVI_{Max} - NDVI_{Min}) \quad (8)$$

In order to estimate LST, the land surface emissivity LSE (ε) must be determined. This is because the LSE is the efficiency with which thermal energy is transmitted from the surface into the atmosphere, and it is a proportionality factor that scales blackbody radiance (Planck's law) to predict emitted radiance (Dozier & Warren, 1982; Jiménez-Muñoz & Sobrino, 2009). Equation 9 is used to derive the land surface emissivity LSE (ε), as suggested by (Sobrino, & Paolini, 2004; Zanter, 2019).

$$\varepsilon = 0.004P_v + 0.986 \quad (9)$$

Where:

ε=is emissivity and Pv is the proportion of vegetation.

Mono window algorithm for LST estimation

An evaluation of land surface temperature (LST) for 2011 and 2021 using Equation 10 and Landsat 5 and Landsat 8 has been performed using the Mono Window Algorithm.
Land surface temperature

$$(Ts) = BT/1 + W^{\times}(BT/P)^{\times}In(\varepsilon) \quad (10)$$

Where:
BT=brightness (at-satellite temperature)
W=wavelength of emitted radiance (11.5µm)
P=14,380 (constant)

Results and Discussion

Anthropogenic heat rises as urban areas become more built up, with more impervious or concrete surfaces, industrial production units, transportation systems, lesser water bodies and trees, etc. This causes the city

to warm up faster than its outskirts. The urban heat island effect is the result of higher land surface temperatures (LST) in cities compared to the surrounding rural areas (Essa, van der Kwast, Verbeiren, & Batelaan, 2013). The correlation between expanding urban areas and rising urban heat island (UHI) tendencies provides further evidence that urbanization is associated with rising temperatures (Ukwattage & Dayawansa, 2012).

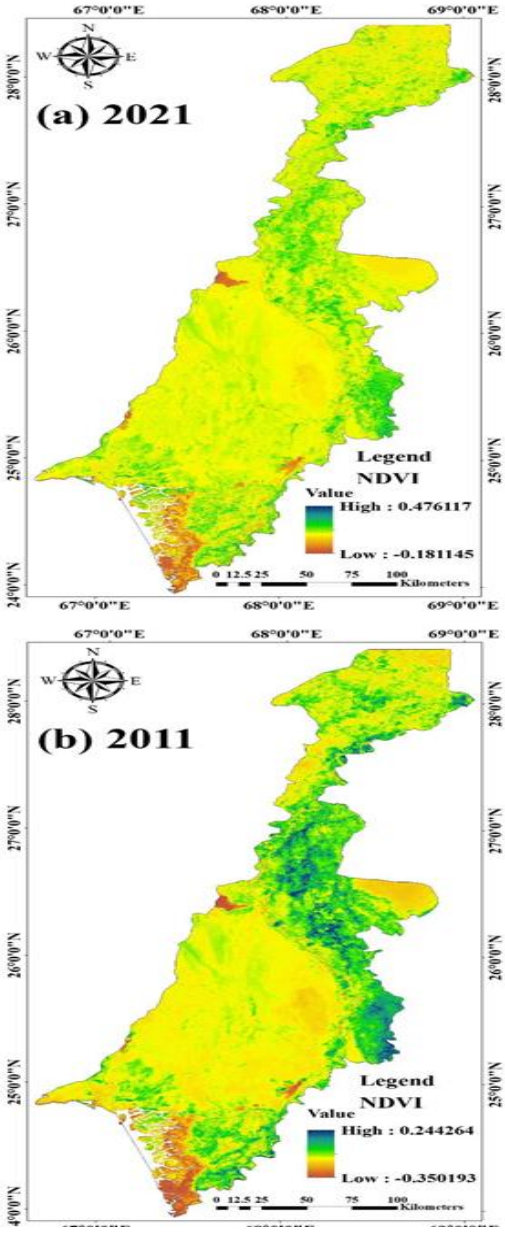

Figure 3. NDVI map of study area (a) 13 May, 2021 and (b) 03 June, 2011.

In this study, the major cities of Sindh's NDVI and LST are calculated, the research work foccused on

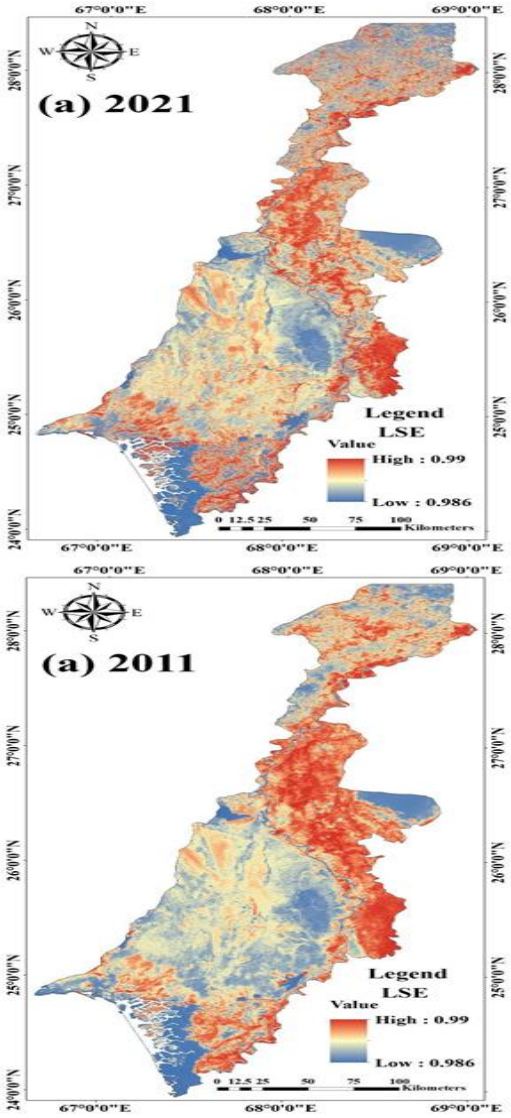

Figure 4. LSE map of study area (a) 13 May, 2021 and (b) 03 June, 2011.

NDVI and LST are computed over the major cities of Sindh. The findings indicate that the NDVI was highest in 2011 and 2021 in the areas that are adjacent to the Indus River in the north, center, south-central, and south, and that the NDVI was lowest in the built-up areas that predominated the residential area in the most advantageous part of the study area. In 2021, NDVI values range from 0.181145 to 0.476117. (Figure 3 (a)). The study area's central region had the lowest NDVI in 2011, ranging from 0.350193 to 0.244264, while higher values were found in the upper northern, eastern, and southern parts. (Figure 3 (b)). Based on these NDVI values, it appears that low-density vegetation, like grassland or shrubs, predominates (Bindi et al. 2009). A value of 0.1 or

lower for the normalised difference vegetation index (NDVI) denotes non-vegetated land, which may be urban or open land area (Figure. 3).

LST Validation

The two primary models used to validate LSTs were derived from either surface-level temperature measurements or data collected from the air just above the ground (Hook, Vaughan, Tonooka, & Schladow, 2007; Z.-L. Li et al., 2013). For example, (Srivastava, Majumdar, & Bhattacharya, 2009) It was discovered that the accuracy of the results in some areas differed by 2 °C from actual ground temperature

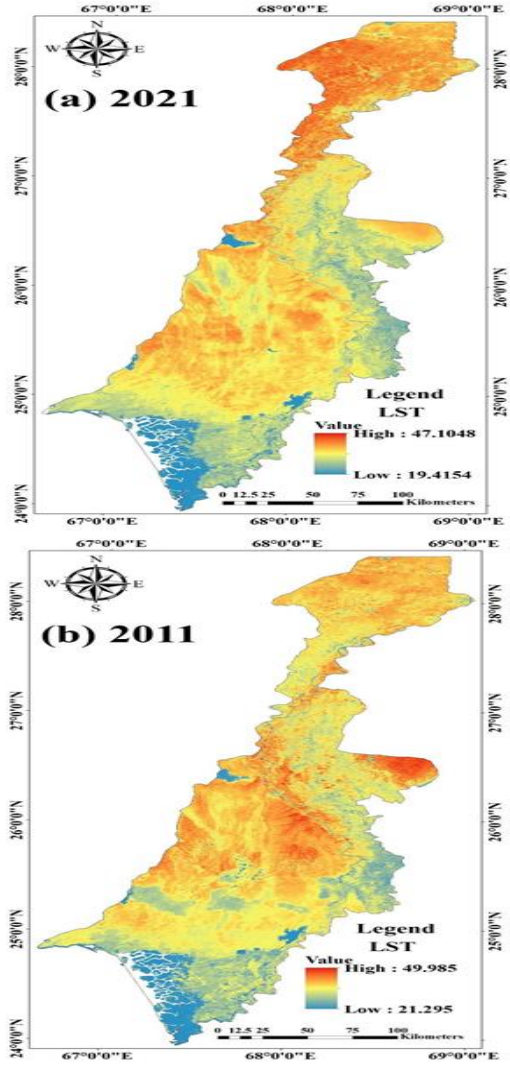

Figure 5. LST map of study area (a) 13 May, 2021 and (b) 03 June, 2011 from Mono-Window algorithm.

measurements, but that this error could be as high as ± 5 °C in most to cases. (Z.-L. Li et al., 2013) found that the LST retrieving error was roughly 0.7 °C when compared to another method that used the average near-surface air temperature to prove the results of the retrieved LST. LST, based on the mono window algorithm maximum, is 49.985 °C in 2011. So, based on an analysis of LST data, we can say that in the central part, north eastern part and the north western part of the study area found higher LST, while the low found in the south, east, and some part of the central area of the study is about 21.295 °C (Figure 5 (b)). LST in the 2021 has higher LST found in the north and central part of the study area is about 47.1048 and the low at the eastern and the southern part of the study area is about 19.4154 °C (Figure 5(a)).

Due to the lack of LST ground measurements in the field, LST was compared with air temperature at each MCS using data obtained from Landsat 5 and Landsat 8. Air temperature comparisons can be complicated because of the difference in resolution between Landsat 5 and Landsat 8, which is 100 m for the thermal band and 30 m for the red and NIR bands. The LST from Landsat 5 during the year 2011 was determined and sampled based on the pixel employed by each weather station displays an extremely consistent relationship between air temperature and LST (Figure 6).

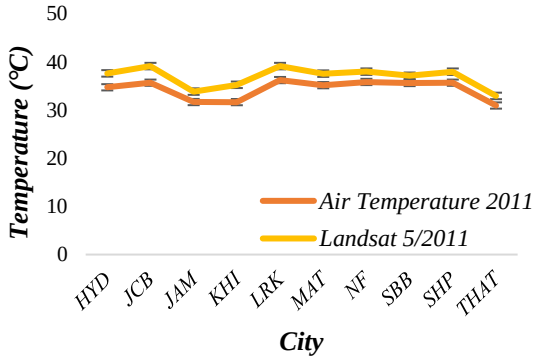

Figure 6. Comparison of air temperature data with Landsat 5 LST on June 3, 2011 at the cities level.

Between Landsat 5 and Landsat 8 data. The LST was generally warmer than the air temperature. Depending on the weather and other relevant factors, the differences can be dramatic at times (Hale, & Yu, 2011). During the time period of 13 May 2021, when the LST from Landsat 8 was compared with data on air temperature, the LST was found to be significantly higher than the air temperature (Figure 7). It is normal and to be expected for there to be differences in the temperatures because there is a difference of 1.1 to 2-m between the temperature of the LST and the temperature of the air. This indicates that variations in the temperatures are to be anticipated and considered to be normal and expected.

Conclusion

This study used the Landsat 5 and Landsat 8 TM, as well as a TIRS sensor, to estimate LST distribution and determine temperature variation in the study area. This data was obtained through remote sensing of the study region. The procedure was utilized in order to derive an estimate of the LST using the TM and TIRS data. The interpretation of the findings suggested that the heat energy radiated by the earth's surface was responsible for determining factors in the study area such as the various types of land use, vegetation cover, soil, and hilly areas. This demonstrated the difference in surface temperature that exists between the various surface patterns. The findings also made it abundantly clear that shifts in surface temperature controlled surface heat and water exchange with the atmosphere, which in turn caused climate change in the region. This was shown to be the case by the findings. This was demonstrated by the findings. Some climatic phenomena have a relatively minor impact on temperature variation, while others have a significant impact. Examples of activities that contribute to deforestation include the replacement of forests with settlements and restaurants, firewood combustion in kitchens, periodic removal of firewood, such as eucalyptus, and rapid tourism development that leads to land conversion. Using data from satellites like Landsat 5 TM and Landsat 8 TM, TIRS can reliably estimate LST. Findings from this study can be used to make educated guesses about the occurrence of extreme weather conditions, including microclimates, hot spots, and high temperatures, can pose a threat to the most vulnerable parts of the research area, as well as to determine whether or not reforestation, frequent vehicle checks for pollution, and reduced plastic incineration are necessary scientific actions to be taken to slow the rate of temperature increase.

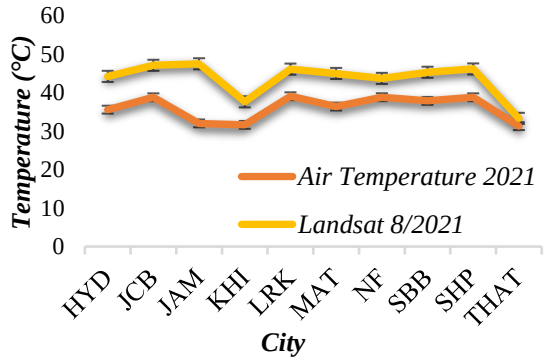

Figure 7. Comparison of air temperature data with Landsat 8 LST on May 13, 2021 at the cities scale.

Acknowledgments

The authors would like to express their gratitude to the United States Geological Survey (USGS) for making available, via the Earth Explorer, the Landsat 5 and Landsat 8 satellite data used in this study. The authors also sincerely thank the knowledgeable reviewers for their helpful suggestions, which have significantly improved the paper. This research paper is dedicated to Dr Nazar H Soomro, from 1st Jan 1975- 21st Jan 2012, (Educational Psychologist University of Sindh).

References

Allen, M. R., Dube, O. P., Solecki, W., Aragon-Durand, F., Cramer, W., Humphreys, S., . Mulugetta, Y. (2018). Chapter 1 Framing and Context. *Global warming of, 1*.

Awuh, M., Japhets, P., Officha, M., Okolie, A., & Enete, I. (2019). A correlation analysis of the relationship between land use and land cover/land surface temperature in Abuja Municipal, FCT, Nigeria. *Journal of Geographic Information System, 11*(01), 44.

Brown, S., Lugo, A. E., & Chapman, J. (1986). Biomass of tropical tree plantations and its implications for the global carbon budget. *Canadian Journal of Forest Research, 16*(2), 390-394.

Cao, L., Li, P., Zhang, L., & Chen, T. (2008). Remote sensing image-based analysis of the relationship between urban heat island and vegetation fraction. *The International Archives of the Photogrammetry, Remote Sensing and Spatial Information Sciences, 37*, 1379-1384.

Dagliyar, A., Avdan, U., Demircioglu Yildiz, N., & Nefeslioglu, H. A. (2015). *Determination of land surface temperature by using Landsat 8 TIRS: A case study in Erzurum, Turkey*. Paper presented at the EGU General Assembly Conference Abstracts.

DE JESUS, J. B., & SANTANA, I. D. M. (2017). Estimation of land surface temperature in caatinga area using Landsat 8 data. *Journal of Hyperspectral Remote Sensing, 7*(3), 150-157.

Dozier, J., & Warren, S. G. (1982). Effect of viewing angle on the infrared brightness temperature of snow. *Water resources research, 18*(5), 1424-1434.

Duveiller, G., Hooker, J., & Cescatti, A. (2018). The mark of vegetation change on Earth's surface energy balance, Nat. Commun., 9, 679. In.

Essa, W., van der Kwast, J., Verbeiren, B., & Batelaan, O. (2013). Downscaling of thermal images over urban areas using the land surface temperature–impervious percentage relationship. *International Journal of Applied Earth Observation and Geoinformation, 23*, 95-108.

Gao, B.-C. (1996). NDWI—A normalized difference water index for remote sensing of vegetation liquid water from space. *Remote sensing of environment, 58*(3), 257-266.

Giannini, M., Belfiore, O., Parente, C., & Santamaria, R. (2015). Land Surface Temperature from Landsat 5 TM images: comparison of different methods using airborne thermal data. *Journal of Engineering Science & Technology Review, 8*(3).

Hale, R. C., Gallo, K. P., Tarpley, D., & Yu, Y. (2011). Characterization of variability at in situ locations for calibration/validation of satellite-derived land surface temperature data. *Remote Sensing Letters, 2*(1), 41-50.

Hokao, K., Phonekeo, V., & Srivanit, M. (2012). Assessing the impact of urbanization on urban thermal environment: A case study of Bangkok Metropolitan. *International Journal of Applied, 2*(7).

Hook, S. J., Vaughan, R. G., Tonooka, H., & Schladow, S. G. (2007). Absolute radiometric in-flight validation of mid infrared and thermal infrared data from ASTER and MODIS on the Terra spacecraft using the Lake Tahoe, CA/NV, USA, automated validation site. *IEEE Transactions on Geoscience and Remote Sensing, 45*(6), 1798-1807.

Jarchow, C. J., Nagler, P. L., & Glenn, E. P. (2017). Greenup and evapotranspiration following the Minute 319 pulse flow to Mexico: An analysis using Landsat 8 Normalized Difference Vegetation Index (NDVI) data. *Ecological engineering, 106*, 776-783.

Jiménez-Muñoz, J. C., & Sobrino, J. A. (2009). A single-channel algorithm for land-surface temperature retrieval from ASTER data. *IEEE Geoscience and Remote Sensing Letters, 7*(1), 176-179.

Kumari, B., Tayyab, M., Mallick, J., Khan, M. F., & Rahman, A. (2018). Satellite-driven land surface temperature (LST) using Landsat 5, 7 (TM/ETM+ SLC) and Landsat 8 (OLI/TIRS) data and its association with built-up and green cover over urban Delhi, India. *Remote Sensing in Earth Systems Sciences, 1*(3), 63-78.

Li, F., Jackson, T. J., Kustas, W. P., Schmugge, T. J., French, A. N., Cosh, M. H., & Bindlish, R. (2004). Deriving land surface temperature from Landsat 5 and 7 during SMEX02/SMACEX. *Remote sensing of environment, 92*(4), 521-534.

Li, Z.-L., Tang, B.-H., Wu, H., Ren, H., Yan, G., Wan, Z., . . . Sobrino, J. A. (2013). Satellite-derived land surface temperature: Current status and perspectives. *Remote sensing of environment, 131*, 14-37.

Lv, Z.-q., & Zhou, Q.-g. (2011). Utility of Landsat image in the study of land cover and land surface temperature change. *Procedia environmental sciences, 10*, 1287-1292.

Makinde, E., & Obigha, A. (2017). Comparison between Landsat 7 Enhanced Thematic Mapper Plus (ETM+) and Landsat 8 Operational Land Imager (OLI) Assessment of Vegetation Indices. *Nigerian Journal of Environmental Sciences and Technology (NIJEST) Vol, 1*(2), 355-366.

Mauree, D., Naboni, E., Coccolo, S., Perera, A. T. D., Nik, V. M., & Scartezzini, J.-L. (2019). A review of assessment methods for the urban environment and its energy sustainability to guarantee climate adaptation of future cities. *Renewable and Sustainable Energy Reviews, 112*, 733-746.

Ning, J., Gao, Z., Meng, R., Xu, F., & Gao, M. (2018). Analysis of relationships between land surface temperature and land use changes in the Yellow River Delta. *Frontiers of earth science, 12*(2), 444-456.

Sekertekin, A., & Bonafoni, S. (2020). Land surface temperature retrieval from Landsat 5, 7, and 8 over rural areas: Assessment of different retrieval algorithms and emissivity models and toolbox implementation. *Remote Sensing, 12*(2), 294.

Sobrino, J. A., Jiménez-Muñoz, J. C., & Paolini, L. (2004). Land surface temperature retrieval from LANDSAT TM 5. *Remote sensing of environment, 90*(4), 434-440. Srivastava, P., Majumdar, T., & Bhattacharya, A. K. (2009). Surface temperature estimation in Singhbhum Shear Zone of India using Landsat-7 ETM+ thermal infrared data. *Advances in Space Research, 43*(10), 1563-1574.

Suga, Y., Ogawa, H., Ohno, K., & Yamada, K. (2003). Detection of surface temperature from Landsat-7/ETM+. *Advances in Space Research, 32*(11), 2235-2240.

Ukwattage, N., & Dayawansa, N. (2012). Urban heat islands and the energy demand: an analysis for Colombo City of Sri Lanka using thermal remote sensing data. *International Journal of Remote Sensing and GIS, 1*(2), 124-131.

Wulder, M. A., Loveland, T. R., Roy, D. P., Crawford, C. J., Masek, J. G., Woodcock, C. E., . . . Cohen, W. B. (2019). Current status of Landsat program, science, and applications. *Remote sensing of environment, 225*, 127-147.

Yu, Y., Tarpley, D., Privette, J. L., Flynn, L. E., Xu, H., Chen, M., . . . Tian, Y. (2011). Validation of GOES-R satellite land surface temperature algorithm using SURFRAD ground measurements and statistical estimates of error properties. *IEEE Transactions on Geoscience and Remote Sensing, 50*(3), 704-713.

Zanter, K. (2019). LANDSAT 8 (L8) Data Users Handbook (LSDS-1574 Version 5.0). *United States Geological Survey: Sioux Falls, SC, USA*.